J Mater Sci: Mater Med (2009) 20:573–581
DOI 10.1007/s10856-008-3565-4

Bioactivity of gelatin coated magnetic iron oxide nanoparticles: in vitro evaluation

Babita Gaihre · Myung Seob Khil · Hyo Kyoung Kang · Hak Yong Kim

Received: 14 March 2008 / Accepted: 14 August 2008 / Published online: 7 October 2008

Abstract Current research explores formation of bone like apatite on gelatin coated magnetic iron oxide nanoparticles (GIOPs) to evaluate the bioactivity of the material. The GIOPs were soaked in simulated body fluid (SBF) and the apatite formation on the surface was investigated in regular interval of time. Fourier transform-infrared (FT-IR) and x-ray diffraction spectroscopic (XRD) analyses were done to investigate the chemical changes and field emission-scanning electron microscopic (FE-SEM) analysis was done to investigate the morphological changes occurring on the surface of the GIOPs after soaking in different time intervals. The kinetic studies of the apatite growth in SBF suggest that initially calcium and phosphorous ions were deposited to the surface of the GIOPs from the SBF leading to formation of amorphous Ca/P particles. Later, after 9 days of the incubation the amorphous particles were fused to form needle and blade like crystalline structures of bone like apatite.

1 Introduction

Estimated deaths from cancer of the bones and joints in the United State in 2008 are 1,470 according to research from National Cancer Institute and surgery, chemotherapy, radiation therapy, immunotherapy, hyperthermia, etc. are some of the current methods of treatment. Hyperthermic treatment of cancer consists of heating tumors upto temperature 43–47°C. The cancer cells are selectively destroyed in this range of temperature while the healthy cells undergo only small reversible damage. However, the main drawback of this method is the difficulty for reaching and controlling the temperature at the tumor site. One alternative might be the use of magnetic thermoseeds implanted in the cancerous tissue. When an external magnetic field is applied to the area heat is generated due to magnetic particles, which heat and kill the tumor cells.

In recent years, there has been a growing interest for this kind of implants and several types of ferrimagnetic thermoseeds have been developed as potential biomaterials for the hyperthermic treatment of bone cancer cells by adding magnetite (IOPs) in the $CaO–SiO_2–B_2O_3–P_2O_5–SiO_2$ systems [1–3]. These thermoseeds are implanted near the tumor area and heated with the help of external magnetic field. These materials not only allow the hyperthermic treatment but also reinforce the weakened bone. Moreover, utilization of IOPs for various biomedical applications has the advantage that the body is designed to process excess iron. In the human body iron is stored primarily in the core of the iron storage protein ferritin. Iron that is contained in endosomes and lysosomes (post-cell uptake) is known to be metabolized into elemental iron and oxygen by hydrolytic enzymes, where the iron joins normal body stores. Iron homeostasis is well controlled by adsorption, excretion and storage, and thus it is postulated that following the administration of iron nanoparticles, iron in the body can be processed.

However, since these thermoseeds are prepared at high temperature, phase transformation of the IOPs to hematite

B. Gaihre
Department of Bionanosystem Engineering, Chonbuk National University, Chonju 561-756, Republic of Korea

M. S. Khil · H. Y. Kim (✉)
Center for Healthcare Technology Development, Chonbuk National University, Chonju 561-756, Republic of Korea
e-mail: khy@chonbuk.ac.kr

M. S. Khil · H. K. Kang · H. Y. Kim
Department of Textile Engineering, Chonbuk National University, Chonju 561-756, Republic of Korea

(α-Fe_2O_3) occurs [4, 5], which results decrease in heat producing power of the materials [6]. For example, Kawashita et al. found that the heat-producing capacity of the IOPs microspheres prepared at low temperature was 4 times higher compared to those prepared at high temperature [2]. Leventouri and et al. also observed same type of decreased magnetic properties of the ferrimagnetic bioceramics with heat [7].

Above results point towards development of the biomaterials in the less severe conditions so that the magnetic property of the composite materials is preserved and effective heating power can be obtained from least amount of the materials, hence, reducing overall dosages given to patients. Exciting results, indeed, were found in vivo using bone cement prepared under less severe conditions [8].

Polymer coated IOPs could be another alternative to the thermoseeds for the hyperthermic treatment of the cancer cells [9]. Gelatin, which is derived from collagen (the major constituent of human bone) have shown greater affinity for bone tissue and found to be inducing bone formation [10]. So, surface coating of IOPs with gelatin can creates a new type of biomaterial in which special biological functionality of the gelatin (to induce the bone formation) is combined with the heat producing property of the IOPs-core. Furthermore, since the surface coating is done in less drastic environment [11, 12] possibility of phase transformation of IOPs to other non-magnetic form, hence, reduction of heat producing capacity is less.

However, as mentioned before these material should be bioactive i.e. they should be able to create a bond with the host living bone through the formation of a biological active bonelike apatite layer on the surface of the material in contact with physiological fluids. In vitro evaluation of bioactivity of a material is done by soaking the material in the simulated body fluid, a buffer solution with ion content similar to blood, and investigating time dependent formation of bone like apatite on the material [13]. It is believed that the materials forming an apaptite layer on their surfaces in simulated body fluid bond to the bone through the same kind of apatite layer formed in the living body [13].

In this study, in order to evaluate the bioactivity of the material in vitro, the gelatin coated magnetic iron oxide nanoparticles (GIOPs) were soaked in simulated body fluid and apatite formation on the surface was investigated in regular interval of time. The FT-IR and XRD analyses were done to investigate the chemical changes and FE-SEM analysis was done to investigate the morphological changes occurring on the surface of the GIOPs after soaking in different time intervals. Appearance of needle shaped type B carbonated apatite in 12 days from the GIOPs indicates the bioactivity of the material.

2 Materials and methods

The starting materials were gelatin type B from bovine skin ($\sim$225 bloom, sigma-aldrich, USA), iron (III) chloride hexahydrate ($FeCl_3 \cdot 6H_2O$, fisher scientific, UK), iron (II) chloride tetrahydrate ($FeCl_2 \cdot 4H_2O$, fisher scientific, UK), sodium hydroxide (NaOH, fisher scientific, UK). Deionized water purged with nitrogen gas was used in all steps involved.

2.1 Synthesis of magnetite nanoparticles (IOPs)

The magnetite nanoparticles (IOPs) were prepared using previously reported method [14]. Briefly, iron ion solution with Fe(II)/Fe(III) = 0.5 molar ratio was prepared by dissolving 5.4 g $FeCl_3 \cdot 6H_2O$ and 2 g $FeCl_2 \cdot 4H_2O$ in 60 ml 0.16 M aq. HCl. The resulting solution was added dropwise into 100 ml of 1 M aq. NaOH with vigorous stirring under inert atmosphere of nitrogen gas. Stirring of the solution was continued for further 30 min and the particles were recovered by centrifugation at 5,000 rpm. The purification steps involved washing repeatedly with deionized water and collecting by centrifugation until supernatant liquid showed neutral pH. After washing, the particles were vacuum dried.

2.2 Surface coating of IOPs with gelatin

Surface coating of the IOPs with gelatin B was done by previously reported methods [11, 12]. Briefly, 0.5 g Fe_3O_4 was dispersed in 250 ml 0.8% (w/v) gelatin solution with brief sonication for 10 s. The dispersion was, then, incubated for 24 h at 37°C. The stable colloidal dispersion was collected after discarding aggregated particles and the gelatin coated magnetic iron oxide nanoparticles (GIOPs) were collected using a magnet.

2.3 Effect of pH and salinity on the gelatin adsorption to the IOPs surface

To see the effect of pH and salinity on the gelatin adsorption to the IOPs surface the IOPs and gelatin solution were incubated under different conditions of pH and salinity. At the end of incubation, the particles were collected with magnet and percentage of gelatin adsorbed to the IOPs surface was estimated using thermogravimetric analyzer (Pyris 1 TGA, Perkin, Eimer, USA), operating at a heating rate of 10°C min^{-1} from room temperature to 700°C under steady flow of nitrogen gas was used to measure the amount the gelatin adsorbed to the surface of the IOPs [11, 12].

The effect of pH was studied by incubating the dispersions at 37°C in the pH range 4–8 for 24 h. pH of

dispersion was adjusted by adding 0.1 M HCl or 0.1 M NaOH. The effect of ionic concentrations (0.05, 0.1, and 0.5 molar NaCl) was studied by incubating the dispersions at 37°C in pH 5 for 24 h. The appropriate amount of NaCl was added to the dispersion to obtain the given concentrations.

2.4 Characterization of gelatin coated magnetic iron oxide nanoparticles (GIOPs)

The functional groups analysis of the samples was done using fourier transform-infrared spectroscopy (FT-IR, FTS 1000, Varian, USA). X-ray diffractometer (XRD, Lad-X 600, Shimadzu, Japan) utilizing CuKα radiation (λ = 1.54053 A), operating at 30 mA and 40 kV, was used to investigate the crystalline phases. The scan rate and scan angle were fixed at 4° min^{-1} and 20–70 2θ°, respectively. The size and morphology of the samples were analyzed using transmission electron microscopy (BIO-TEM, H-7650, Hitachi, Japan), operating at 100 kV and field emission-scanning electron microscopy (FE-SEM, S-4700, Hitachi, Japan), operating at 10 kV.

2.5 In vitro bioactivity assessment

The in vitro bioactivity study of the GIOPs was done by soaking 10 mg GIOPs in 50 ml simulated body fluid (SBF) for 3–21 days in plastic tubes and investigating formation of the bone-like apatite on the surface [15, 16]. The SBF solution was prepared using previously described method [17]. The salt components viz. NaCl, $NaHCO_3$, KCl, K_2HPO_4, $MgCl_2 \cdot 6H_2O$, HCl, $CaCl_2$, Na_2SO_4, and $(CH_2OH)_3CNH_2$ were added in the same order as described in the reference to give the ionic concentration of human plasma. The FE-SEM images were used to investigate morphological changes occurring after the in vitro experiment. The calcium to phosphorus ratio (Ca/P) of the samples was calculated using energy dispersive x-ray analyzer (EDX, JSM-6400, JEOL, Japan). The kinetic of the apatite development on the surface of the samples was monitored using XRD, FT-IR, and inductively coupled plasma spectrometer (ICPS-7500, Shimadzu, Japan).

3 Results and discussion

3.1 Surface coating of IOPs with gelatin

Gelatin being a protein is made up of amino acids (Scheme 1a). Each of the amino acids is joined by peptide bonds between the carbonyl and amino groups of adjacent amino acid residue forming a linear chain. The linear chains are held together by H-bond leading to formation of complex secondary and tertiary structure [18]. Due to electron-withdrawing nature of the carbonyl groups in each amino acid groups and due to presence of the lone pair of

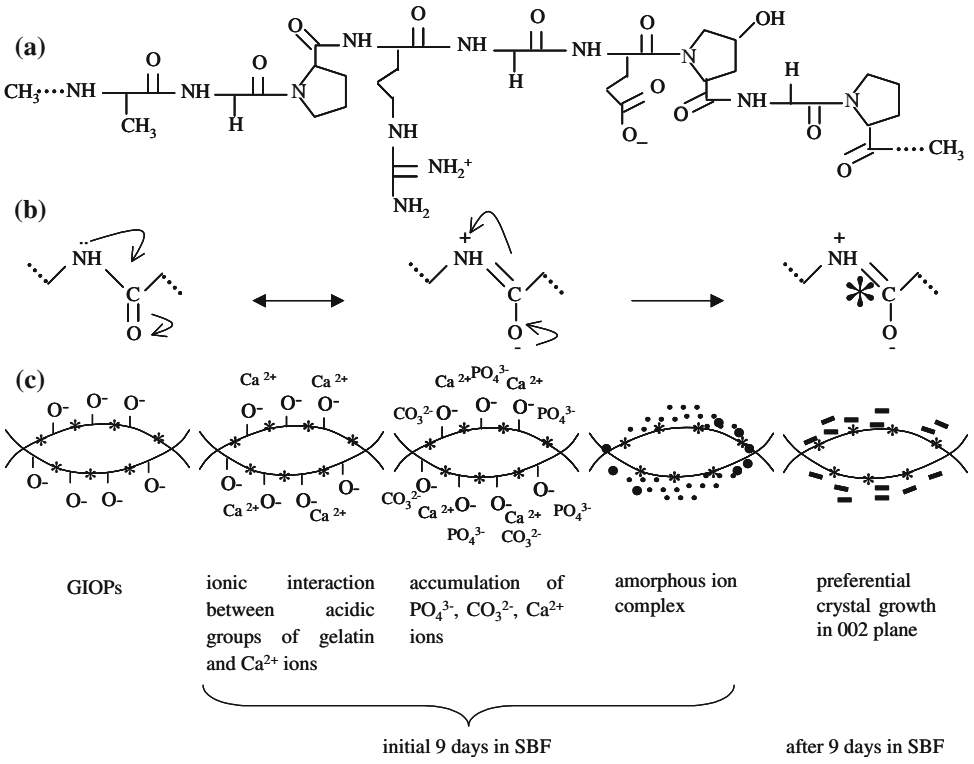

Scheme 1 Chemical structure of gelatin (**a**), adsorption of IOPs (*) to the amide bonds of gelatin (**b**), and mechanism of apatite growth on the surface of GIOPs in the physiological condition (**c**)

electrons on the nitrogen of the amide groups, the charge delocalization by resonance is possible leading to development of negative, positive or neutral charge in the gelatin chain depending upon the pH of the solution. Such charge delocalization is possible due to presence of carboxylic groups also [10]. The pH of the gelatin solution was around 5.2 i.e. around its isoelectric point so we can expect neutral or slightly negative charge on the gelatin chain.

On the other hand, in an aqueous system IOPs are coordinated with water molecules, which share their electron pairs with iron atom. Upon adsorption, the water molecules usually dissociate resulting in a surface covered by hydroxyl groups coordinated to the underlying iron atoms [19]. The hydrous iron oxides have amphoteric characteristics that can act as positive ($FeOH^{2+}$) site and interact with lone pair of electrons present in nitrogen atoms of amine groups and/or anionic carbonyl oxygen in acidic medium [20] or act as negative (FeO^{-}) site and interact with electron deficient groups in basic or neutral medium [19]. In present study, the IOPs were washed to neutral pH and dispersed in gelatin solution at pH 5 positive charge can be expected on the IOPs surface [19].

The isoelectric point of each of the components along with the corresponding charge in different pH is summarized in Table 1. The table can be used to predict the adsorption behavior of gelatin and IOPs. According to the table, at pH 4 both of the reacting components would be positively charged, hence, the adsorption would be unfavorable due to electrostatic repulsion between the like charges. Same conclusion can be made for the adsorption at higher pH. However at pH 5 and 6, the table predicts the favorable electrostatic interactions. So, it is logical to assume that at the given condition of pH, in our experiment, first stage adsorption might occur due to electrostatic interaction between the positively charge IOPs and negatively charged gelatin chain as shown in Scheme 1b.

The dependence of adsorption phenomenon on pH and ionic concentration of the medium shown in the Fig. 1 supports the above logic. The figure shows larger amount of gelatin adsorbed to the IOPs at pH 5 but the amount decreases with increasing the pH from 7 to 8. Similarly, the adsorption was found to be lower at pH 4.5. Also, the adsorption of gelatin was found to decrease with increasing ionic concentrations of the medium (Fig. 1b) because presence of salt in the solution definitely blocks the sites of interactions, hence, reducing the adsorption phenomenon. From the Fig. 1 conclusion can be made that electrostatic interaction is involved in the adsorption phenomenon of IOPs and gelatin. However, further adsorption of the gelatin chain is possible due to the hydrophobic interaction as suggested by Rolf et al. [20].

The Fig. 2A represents the FT-IR spectrum of the GIOPs along with plain gelatin and IOPs. The peaks at 580 and 400 cm^{-1} are the characteristic peaks for the IOPs [6, 21]. Similarly, the plain gelatin exhibits a number of characteristic spectral bands (Fig. 2A-b). The most characteristics of them are; N–H stretching at 3,300–3,500 cm^{-1} for amide A, C–H stretching at 3,064 cm^{-1} for amide B, C=O stretching at 1,670 cm^{-1} for amide I, N–H deformation at 1,560 cm^{-1} for the amide II, and other bands associated with C–N stretching and N–H deformation for amide III groups [18]. All these characteristic bands are present in the spectrum for GIOPs too (Fig. 2A-c). Moreover, the characteristic bands for IOPs are also seen in their usual positions at 580 and 400 cm^{-1}. However, after coating the band positions for amide I and II are shifted to 1,642 and 1,533 cm^{-1}, respectively, as well as broadness of the band in amide A region is also decreased significantly. The vibrational frequency of carbonyl band of amide I, in proteins, is found to be dependant on the hydrogen bonding between amide units, leading to development of the

Table 1 Isoelectric point and corresponding charges on the IOPs and gelatin in different pH

pH	IOP spI 6.7[a]	Gelatin B pI 4.7–5.2[b]
4	+	+
5	+	0
6	+	−
7–8	−	−

[a] Ref no. 19

[b] Supplier data

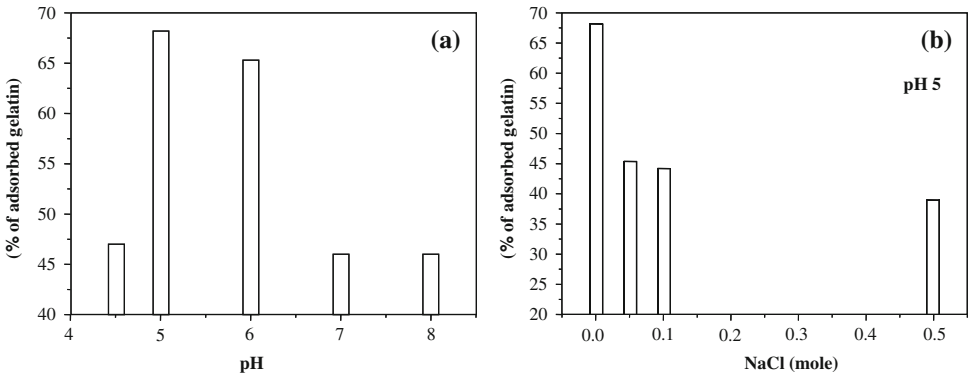

Fig. 1 Effect of pH (**a**) and ionic concentration (**b**) on the gelatin adsorption to the IOPs

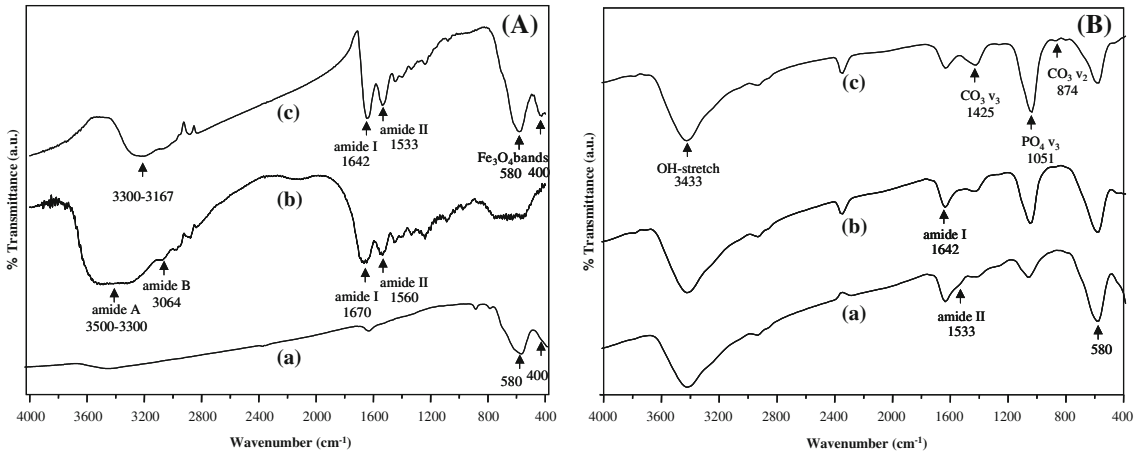

Fig. 2 FT-IR spectra of IOPs (a), gelatin (b), and GIOPs (c) (**A**), and GIOPs after 6 (a), 15 (b), and 21 (c) days of soaking in SBF (**B**)

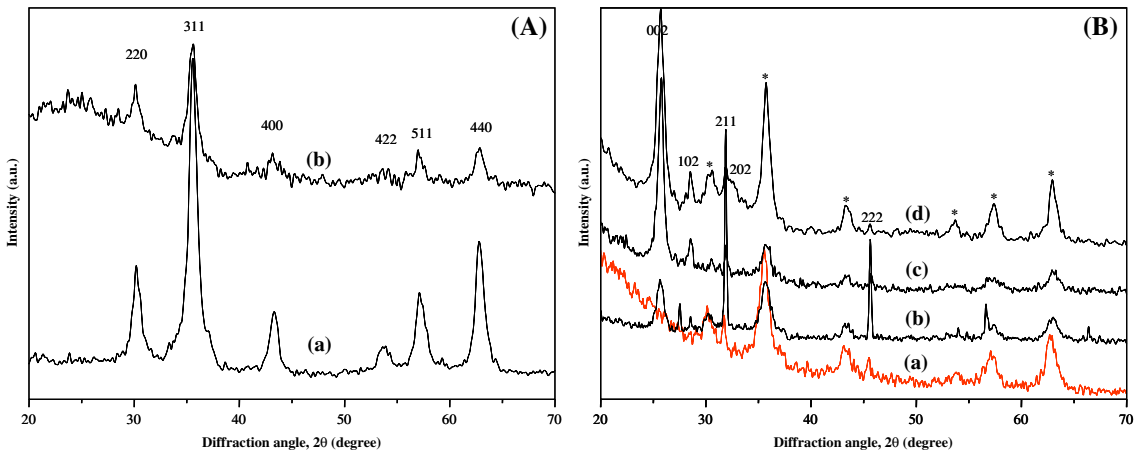

Fig. 3 XRD patterns of IOPs (a) and GIOPs (b) (**A**), GIOPs after 3 (a), 12 (b), 15 (c), and 21 (d) days of soaking in SBF (**B**). Asterisk in the figure represent the peak positions of IOPs

secondary structure. The red shifting of the amide bands might be the result of changes in peptide secondary structure due to adsorption of the IOPs to the amide bonds. Same conclusion can be drawn from the decreased broadness of the band in amide A region [18]. The FT-IR analysis suggests some type of interaction between IOPs and gelatin molecules. From Figs. 1 and 2 conclusion can be made that electrostatic as well as other types of interaction might be involved in the adsorption of gelatin chain to the IOPs.

The crystalline phases of the GIOPs were characterized by observing XRD patterns of the sample (Fig. 3A). The positions and relative intensities of the peaks at 2θ angles of 30.1 ($d = 0.296$ nm), 35.5 ($d = 0.252$ nm), 43.3 ($d = 0.208$), 53.4 ($d = 0.171$), 56.4 ($d = 0.1628$), and 62.6 ($d = 0.148$), are quite similar to those of IOPs [5]. Presence of oxygen can lead to oxidation of IOPs to haematite, ferric hydroxide and other phase of iron oxides [4]. The xrd patterns ruled out presence of all these unwanted impurities.

Morphology and size analyses of the GIOPs were done using FE-SEM and BIO-TEM techniques. The FE-SEM image shows spherical morphology with narrow size distribution (Fig. 4a). The true internal structure of the composite nanoparticles can be visualized by TEM because the IOPs can absorb electric beam appear as dark spots in the TEM image. Since, there are many binding sites (i.e., amide groups, as shown by FT-IR analysis) for IOPs per gelatin chain (Scheme 1a and b), TEM reveals the clusters with each cluster carrying spherical nanoparticles of size about 8 nm (Fig. 4b). It looks like when IOPs are dispersed in the aqueous solution of gelatin, they are adsorbed to the gelatin chain due to electrostatic interaction and polymeric chain protects each cluster of the IOPs from aggregation. The selected area diffraction pattern (SADP) of the composite shows the characteristic diffraction ring for IOPs (Fig. 4c). The FT-IR, TGA, XRD, FE-SEM and BIO-TEM along with SADP analysis of the GIOPs suggest surface modification of IOPs with gelatin.

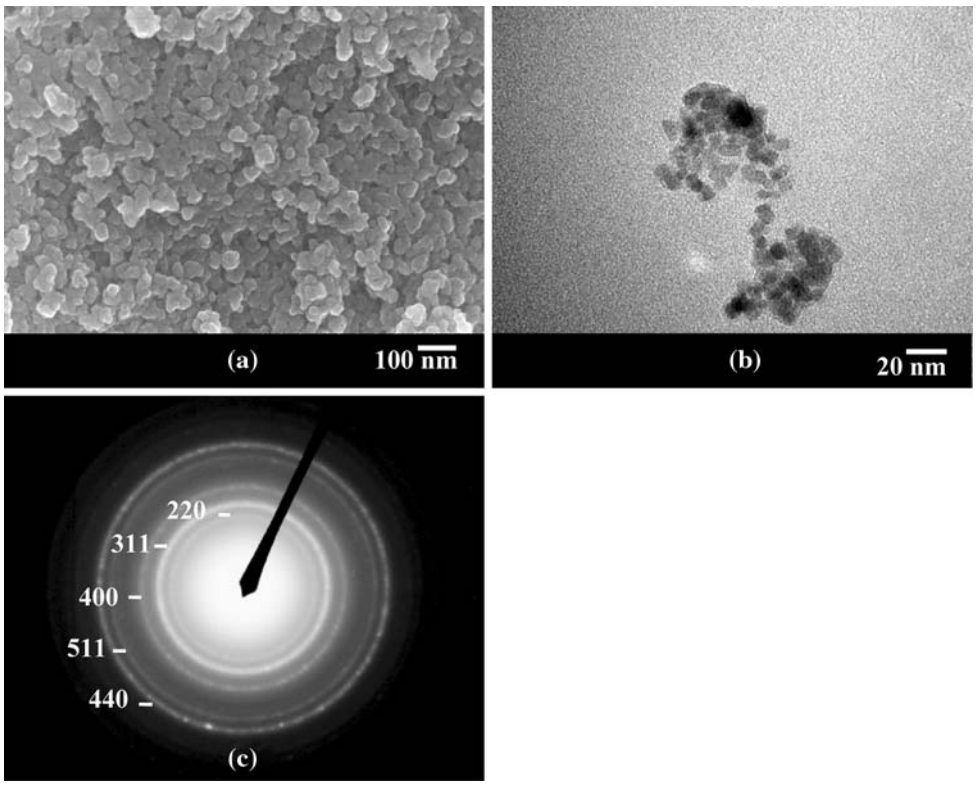

Fig. 4 FE-SEM (**a**), BIO-TEM (**b**), and selected area diffraction patterns (**c**) of GIOPs

3.2 In vitro bioactivity assessment

Appearance of 002 and 211 phases in the XRD spectra of the SBF soaked samples, within 2 or 3 weeks, is taken as an indication of the bioactivity of material [15, 16, 22]. Figure 3B represents the XRD patterns of the GIOPs after soaking in the SBF for various intervals. The peak assignments in the XRD spectrum were done according to the previously reported references [15, 16, 22]. The figure shows appearance of 211 phase at 32 2θ° after 3 days of soaking. Similar patterns of peaks were seen in the samples upto 9 days, after which extra peaks appeared at 26 and 28 2θ°, corresponding to 002 and 102 phases. Similarly, an extra peak can be seen at 46 2θ, which can be assigned as 222 phase [JCPDS, card no. 09-0432]. Furthermore, on increasing the soaking time to 21 days broadness of the peak at 32 2θ° was increased. It appears that the increase in the broadness is due to appearance and merger of the new peak at 34 2θ°, attributing to 202 phase, with the peak at 32 2θ°.

The figure also shows that the intensity of the 211 peak was extremely high for the GIOPs soaked in SBF for 12 days (Fig. 3B), but decreased remarkably after the soaking in SBF for 15 days. On the other hand, in GIOPs soaked in SBF for 12 days, the remarkable peak at 46 in 2θ° was also observed. This peak decreased after the soaking in SBF for 15 days, similarly to the peak at 32°. It appears that the XRD peak at 32° is closely related with the one at 46°. Such an increase (or decrease) in XRD peaks relative to other peaks (especially 002 and 211) are seen in other cases also [23], however, such correlation between 222 and 211 phases is not yet reported and is subject of further study. Nevertheless, appearance of all the peaks on the specified positions indicates the bioactivity of the GIOPs. Moreover, gradual increase in the intensity of peak at 26 2θ°, with increasing time of soaking, indicates crystal growth occurring preferentially to 002 plane.

FT-IR studies of the calcified tissue shows PO_4^{3-} bands at 500–600 and 900–1,225 cm^{-1}, and various other peaks associated with CO_3^{2-} depending upon labile, type A, and type B carbonated apatites [24]. Presence of the bands in FT-IR spectra from respective PO_4^{3-} (at 1,051 cm^{-1}) and CO_3^{2-} groups (at 874, 1,425 cm^{-1}) along with various amide bands of gelatin (Fig. 2B) show close resemblance of the material with the real bone [24, 25]. Furthermore, the increasing intensity of CO_3^{2-} band at 1,425 cm^{-1} with the increasing soaking time indicates inclusion of more and more CO_3^{2-} ions to the gradually growing apatites. Moreover, presence of the carbonate bands in the specified positions indicates development of type B carbonated apatite i.e. substitution of PO_4^{3-} with CO_3^{2-} ions occurring in the growing apatite. The increase of calcium to phosphorus (Ca/P) ratio with increasing days of incubation is as expected for such substitution [26]. The Ca/P ratio matches with the natural bone (Ca/P = 1.64) on the 15th day of soaking after which it goes higher and higher as

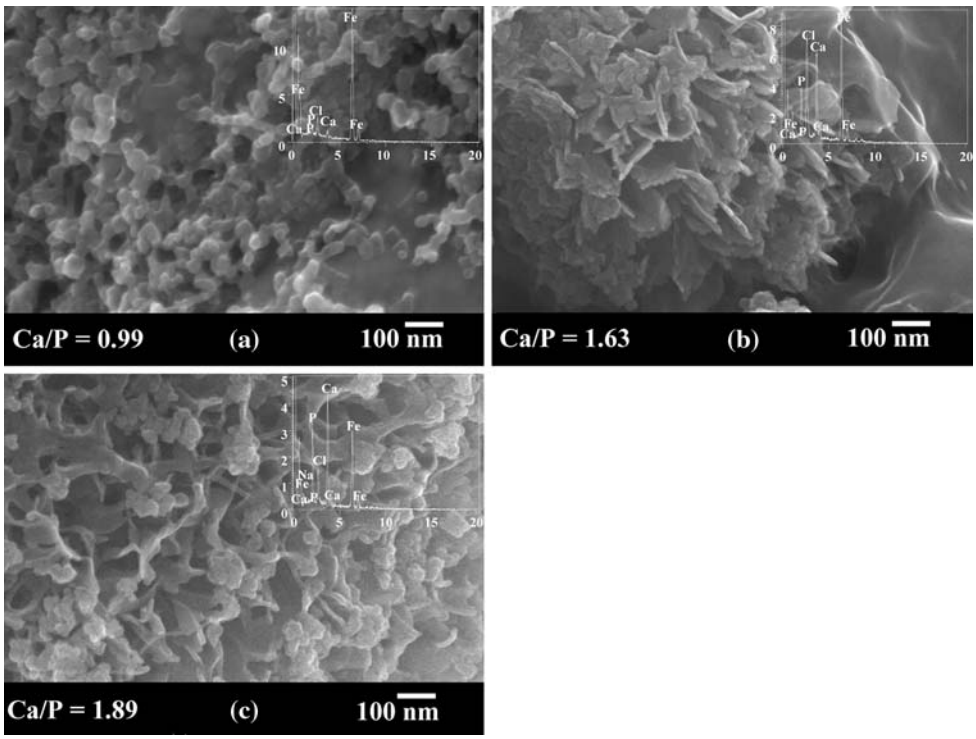

Fig. 5 FE-SEM images, with EDX images in inset, of GIOPs after 3 (**a**), 15 (**b**), and 21 (**c**) days of soaking in SBF

shown by Fig. 6d. The characteristic IOPs peaks appear in their usual positions at 580 and 400 cm^{-1}.

The morphology of the GIOPs after soaking in the SBF was analyzed using FE-SEM (Fig. 5). The surface morphology of the particles, after 3 days of incubation, does not show significant difference from the control sample (Figs. 4a and 5a). They are more or less spherical shape even after 3 days of incubation. However, the corresponding FE-SEM image of the composite particles shows development of the needle and blade like structures after 15 days with Ca/P ratio nearly equal to 1.64. The elongated needle and blade like structure become more prominent with increasing days of incubation (Fig. 5c) and corresponding Ca/P ratio also increases accordingly. The morphology looks like crystals are stacked one above another to give blade like structure. The morphology appears to mimicking the natural bone, which consists of needle shaped crystals entangled in fibrous layer of collagen in regular pattern [10]. These unusual structures developed here might be due to the regulatory function of gelatin molecules to direct the crystal growth in preferential orientation. Furthermore, increasing intensity of calcium and phosphorous compared to iron, with increasing days of soaking, in EDX spectra (Fig. 5, in inset), indicates deposition of the apatite on the surface of GIOPs. From the XRD, FT-IR, and EDX results, we can conclude that the needle and blade like morphologies seen in the FE-SEM images are due to development of type B carbonated apatite like layer.

3.3 Kinetic and mechanism of the apatite growth

The kinetics and mechanism of the apatite growth on the surface of the GIOPs, in the physiological condition, was studied using FT-IR, XRD, ICP, and EDX analysis techniques. The Fig. 6a represents the relative FT-IR peak intensities of PO_4^{3-} (1,051 cm^{-1}) and CO_3^{2-} (1,425 cm^{-1}) of apatite to IOPs (580 cm^{-1}) groups with increasing days of soaking. Similarly, Fig. 6b represents the relative XRD peak intensities of 002 and 211 planes of apatite to 311 plane of IOPs with increasing days of soaking. Faster increasing relative intensity of PO_4^{3-} for the initial 9 days as shown in Fig. 6a, indicates increasing amount of the PO_4^{3-} groups being precipitated in the GIOPs from SBF. Similarly, the decrease in Ca^{2+} ions concentration in SBF indicates simultaneous precipitation of the ions too (Fig. 6c). However, Fig. 6b shows constant relative intensity upto 9 days for, both, 002 and 211 planes. These results suggest formation of only amorphous Ca/P particles in the initial 9 days. This finding is, further, supported by the low Ca/P ratio, which is characteristic of the amorphous nature of the apatite (Fig. 6d). However, after 9 days the Fig. 6b shows increasing intensities with increasing soaking time for, both, 002 and 211 peaks suggesting increasing crystallinity of the growing crystals. Furthermore, the increase in the relative intensity is more for 002 compared to 211 plane, which indicates that the crystal is growing preferentially to the 002 plane. The increase in intensities of PO_4^{3-} and CO_3^{2-} in Fig. 6a, and the decrease

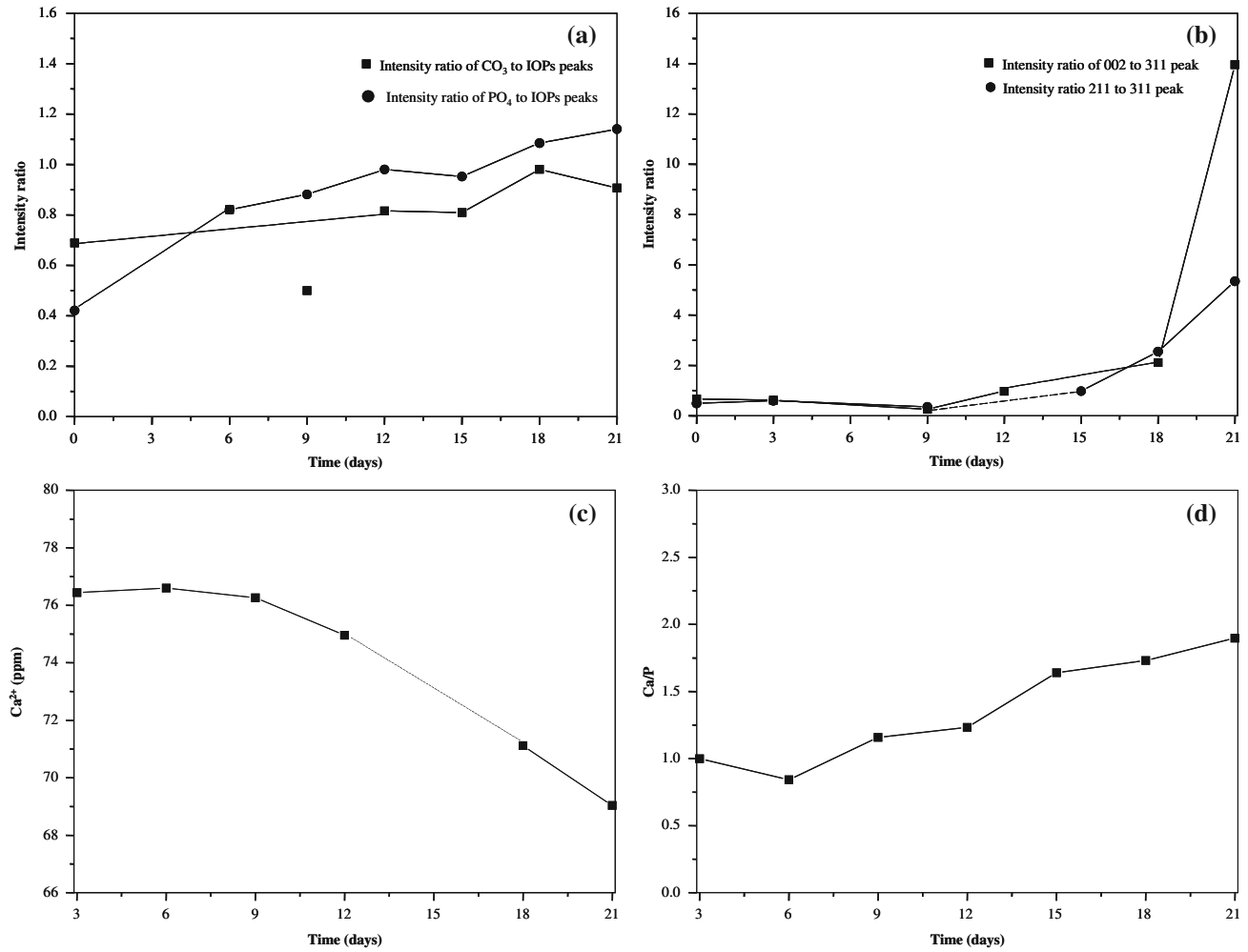

Fig. 6 Relative (FT-IR) intensities of PO_4^{3-} and CO_3^{2-} peaks of apatite to IOPs peaks (**a**), Relative XRD intensities of 002 and 211 peaks of apatite to 311 peak of IOPs (**b**), decreasing Ca^{2+} ion concentrations in SBF (**c**), and increasing Ca/P ratios (**d**), with increasing days of incubation

in Ca^{2+} ion concentration in SBF after 9 days suggest that the crystal is growing by incorporating these ions from SBF. The Fig. 6a suggests that there is rapid accumulation of PO_4^{3-} initially, but after 9 days it remains constant. The CO_3^{2-} band shows significant increase only after 12 days in Fig. 6a, suggesting incorporation of these ions only after the 12th day of incubation. Furthermore, appearance of CO_3^{2-} band in the specified positions in Fig. 2B and constantly increasing Ca/P ratio in Fig. 6d indicates substitution of PO_4^{3-} with CO_3^{2-} ions in growing apatite to give type B carbonated apatite. The steep nature of curve after 9 days in Fig. 6c suggests faster growth rate of the crystals after 9 days. Depending upon the kinetic study, we can generalize the crystal growing mechanism into two phases as shown in Scheme 1c. The first phase includes slower deposition of Ca^{2+} and PO_4^{3-} ions from SBF to the GIOPs surface to form amorphous ion complex for the initial 9 days followed by faster incorporation of Ca^{2+}, CO_3^{2-}, PO_4^{2-}, etc. ions and gradual development of the crystals to 002 plane in the second phase.

Previous studies on the controlled nucleation and growth of hydroxyapatite crystals from organic template, in vitro, suggest that the negative groups on the surface of organic templates are the nucleation sites. The negative groups exposed in solution tend to enrich the cations, which results in local supersaturation followed by nucleation of crystals [27, 28]. Self-aggregation or assembly of proteins plays a key role in the promotion and/or inhibition of crystal growth by blocking specific faces during biomineralization process. The decrease in intensity for amide II bands at 1,533 cm^{-1} indicates possible involvement of the amides in the electrostatic interaction between Ca^{2+} ions and GIOPs. When GIOPs are kept in SBF, it appears that Ca^{2+} ions from the SBF are attracted to amide bonds, where nucleation will be initiated. Afterward, progressive addition of Ca^{2+}, PO_4^{3-}, CO_3^{2-}, and other ions into the nuclei

leads to development of crystals into the various shape and size that is governed by the template layer. The specific stereochemical arrangement of reactive groups is thought to be the main driving force of regulatory functions seen in gelatin for crystal formation in preferred direction [25]. So, we believe that the driving force for the crystal growth in 002 plane, in our in vitro study, might be due to presence of self-assembling gelatin layer in GIOPs.

4 Conclusions

Formation of bone like apatite from GIOPs confirms the in vitro bioactivity of the material. The apatite formation rate, with comparatibly-improved crystallinity, was found to increase after 9 days. The apatite was type-B carbonate substituted, with poor crystallinity. Different spatial arrangement of the functional groups of gelatin in the GIOPs might be the driving force for the development of the crystal preferentially to 002 plane. The better bioactivity, biocompatibility, along with magnetic materials in it makes this biomaterial a potential candidate for hyperthermic treatment of bone cancer cells.

Acknowledgements This research was supported by the Regional Research Center Program of the Korean Ministry of Education (KRF-2005-211-D00054) and Korean Research Foundation Grant Funded by the Korean Government (MOEHRD) the center for Healthcare Technology Development, Jeonju 561–756, Republic of Korea.

References

1. Y. Ebisawa, F. Miyaji, T. Kokubo, K. Ohura, T. Nakamura, Biomaterials **18**, 1277 (1997). doi:10.1016/S0142-9612(97)00067-7
2. M. Kawashita, M. Tanaka, T. Kokubo, Y. Inoue, T. Yao, S. Hamada et al., Biomaterials **26**, 2231 (2005). doi:10.1016/j.biomaterials.2004.07.014
3. M. Kawashita, H. Takaoka, T. Kokubo, T. Yao, S. Hamada, T. Shinjo, J. Ceram. Soc. Jpn. **109**, 39 (2001)
4. F.S. Yen, W. Chen, J.M. Yang, C.T. Hong, Nano. Lett. **2**, 245 (2002). doi:10.1021/nl010089m
5. R.M. Cornell, U. Schwertmann, *The Iron Oxides: Structures, Properties, Reaction, Occurrences and Uses*, 2nd edn. (Wiley, Weinheim, 2000), pp. 142–278
6. R. Hergt, W. Andra, G.C. d' Ambly, I. Hilger, A.W. Kaiser, U. Richter et al., IEEE Trans. Magn. **34**, 3745 (1998). doi:10.1109/20.718537
7. T.H. Leventoruri, A.C. Kis, J.R. Thompson, I.M. Anderson, Biomaterials **26**, 4924 (2005). doi:10.1016/j.biomaterials.2005.01.017
8. T. Kenji, S. Tetsuya, W. Hiroki, S. Jun, Y. Takashi, M. Seiichi et al., Appl. Biomater. **43**, 210 (1998)
9. A.K. Gupta, M. Gupta, Biomaterials **26**, 3995 (2005). doi:10.1016/j.biomaterials.2004.10.012
10. S. Young, M. Wong, Y. Tabata, A.G. Mikos, J. Control Release **109**, 256 (2005). doi:10.1016/j.jconrel.2005.09.023
11. B. Gaihre, S. Aryal, M.S. Khil, H.Y. Kim, J. Microencaps. **25**, 21 (2007)
12. B. Gaihre, S. Aryal, A.M.B. Nasser, H.Y. Kim, Mat. Sci. Eng. C Bio. S (in press)
13. T. Kokubo, H. Kushitani, S. Sakka, T. Kitsugi, T. Yamamuro, J. Biomed. Mater. Res. **24**, 721 (1990). doi:10.1002/jbm.820240607
14. Y.S. Kang, S. Risbud, J.F. Rabolt, P. Stroeve, Chem. Mater. **8**, 2209 (1996). doi:10.1021/cm960157j
15. D. Arcos, R.P.D. Real, V.M. Regi, Biomaterials **23**, 2151 (2002). doi:10.1016/S0142-9612(01)00346-5
16. F. Balas, M. Kawashita, T. Nakamura, T. Kokubo, Biomaterials **27**, 1704 (2006). doi:10.1016/j.biomaterials.2005.10.004
17. T.A. Cuneyt, Biomaterials **21**, 1429 (2000). doi:10.1016/S0142-9612(00)00019-3
18. M.C. Chang, J. Tanaka, Biomaterials **23**, 4811 (2002). doi:10.1016/S0142-9612(02)00232-6
19. E. Illes, E. Tombacz, J. Colloid Interface Sci. **295**, 115 (2006). doi:10.1016/j.jcis.2005.08.003
20. S.O. Rolf, T.A.R. Mats, Langmuir **10**, 211 (1994). doi:10.1021/la00013a030
21. A.K. Gupta, A.S.G. Curtis, Biomaterials **25**, 3029 (2004). doi:10.1016/j.biomaterials.2003.09.095
22. L. Ren, K. Tsuru, S. Hayakawa, A. Osaka, J. Non-Cryst. Solids **285**, 116 (2001). doi:10.1016/S0022-3093(01)00441-0
23. Y. Ebisawa, T. Kokubo, K. Ohura, T. Yamamuro, J. Mater. Sci. Mater. Med. **4**, 225 (1993). doi:10.1007/BF00122273
24. A. Bigi, E. Boanini, S. Panzavolta, N. Roveri, K. Rubini, J. Biomed. Mater. Res. **59**, 709 (2001). doi:10.1002/jbm.10045
25. M.C. Chang, C.C. Ko, W.H. Douglas, Biomaterials **24**, 2853 (2003). doi:10.1016/S0142-9612(03)00115-7
26. L. Muller, F.A. Muller, Acta Biomater. **2**, 181 (2006). doi:10.1016/j.actbio.2005.11.001
27. J. Gautam, H. Schott, J. Pharm. Sci. **83**, 922 (1994). doi:10.1002/jps.2600830703
28. W. Zhang, S.S. Liao, F.Z. Cui, Chem. Mater. **15**, 3221 (2003). doi:10.1021/cm030080g